https://doi.org/10.5194/essd-2026-337
Preprint. Discussion started: 28 July 2026
© Author(s) 2026. CC BY 4.0 License.

Open Access Earth System Science Data Discussions

CMIP6-MedPlus dataset: climate projections for the Mediterranean region using statistical downscaling

Valeria Todaro[1], Daniele Secci[1], Marco D'Oria[1] and Maria Giovanna Tanda[1]

[1] Department of Engineering and Architecture, University of Parma, Parco Area delle Scienze 181/A, 43124 Parma, Italy

Correspondence to: Valeria Todaro (valeria.todaro@unipr.it)

Abstract. Global climate-model projections are often too coarse to represent the spatial variability required for regional assessments. This study presents CMIP6-MedPlus, an open-access climate projection dataset for an extended Mediterranean region, available at https://doi.org/10.5281/zenodo.17898529 (Todaro et al., 2025). It provides daily precipitation and near-surface air temperature at 0.25° spatial resolution for the period 1985–2100, based on five Coupled Model Intercomparison Project Phase 6 (CMIP6) Global Climate Models (GCMs) and two Shared Socioeconomic Pathways (SSP1-2.6 and SSP3-7.0). CMIP6-MedPlus was generated using a statistical downscaling framework that combines deep learning–based spatial refinement with bias correction. First, a Convolutional Neural Network (CNN)-based method was applied to enhance spatial resolution: ERA5 reanalysis fields were upscaled to the GCM resolution and used to train the CNN to learn the mapping between coarse- and fine-scale representations of the same variable. The trained CNN was then applied to GCM outputs to generate more spatially detailed fields. Second, quantile delta mapping was applied to the CNN-refined fields to correct systematic biases relative to ERA5 while preserving climate change signals. The resulting dataset provides spatially consistent regional climate information suitable for climate-impact across Mediterranean and neighbouring areas and serves as a basis for subsequent refinement at basin and local scales.

1 Introduction

Understanding and projecting future climate change is crucial for informing effective regional and local planning and adaptation strategies. Climate models are essential tools for simulating the Earth's climate system and providing long-term climate projections. The Coupled Model Intercomparison Project Phase 6 (CMIP6; Eyring et al., 2016) represents the most recent fully established initiative designed to coordinate climate model experiments. It brings together a comprehensive dataset of climate projections from a wide range of state-of-the-art Global Climate Models (GCMs), offering a robust foundation for exploring future climate conditions. CMIP6 outputs contribute directly to the latest Intergovernmental Panel on Climate Change (IPCC) assessment reports (AR6, IPCC, 2023) and are increasingly used across the scientific community to assess future climate change impacts and support evidence-based policy decisions.

Although CMIP6 offers unprecedented improvements in climate model capabilities and scenario diversity, its GCM outputs still lack the spatial detail required for local-scale impact studies. To overcome this limitation, downscaling techniques can be used to translate large-scale GCM outputs into more detailed, finer-scale projections. Downscaling generally follows two main approaches: dynamical downscaling and statistical downscaling.

Dynamical downscaling uses Regional Climate Models (RCMs) to simulate climate processes over a regional domain, driven by boundary conditions from GCMs. RCMs represents physical processes at a finer scale, providing detailed depictions of regional climate variability. However, dynamical downscaling is computationally intensive. At present, RCM simulations

https://doi.org/10.5194/essd-2026-337
Preprint. Discussion started: 28 July 2026
© Author(s) 2026. CC BY 4.0 License.

driven by CMIP6 GCMs, such as those produced within the Coordinated Regional Downscaling Experiment (CORDEX; Giorgi and Gutowski, 2015), are still underway (Gutowski Jr. et al. 2016; Katragkou et al., 2024), and their availability still lags behind that of CMIP5-based simulations (Ruti et al. 2016; Jacob et al. 2020).

Statistical downscaling offers an efficient alternative to dynamical downscaling by establishing empirical relationships between large-scale climate variables and local-scale observations. Due to its flexibility and modest computational demands, statistical downscaling has been widely adopted in climate research, and various methodologies have been developed (Wilby et al. 1998; Maraun et al. 2010; Tian et al. 2014; Gutiérrez et al. 2019; Tabari et al. 2021; Labeurthre et al. 2025). Statistical downscaling methods are typically grouped into three main frameworks: Perfect Prognosis (PP), Model Output Statistics (MOS) and Weather Generators (WGs). In the PP approach, statistical relationships are established between observed large-scale atmospheric predictors and observed local climate variables (predictands), where the predictors may include either physically related atmospheric variables or the predictand itself at a coarser spatial scale, according to the concept of "self-predictors" (Widmann et al., 2003; Schmidli et al., 2006). These relationships are subsequently applied to predictors obtained from GCMs to produce downscaled climate projections. In contrast, MOS methods directly transform GCM outputs by statistically relating model-simulated predictors, typically consisting of the same variable as the predictand, to the local observed variable, thereby accounting for systematic model errors within the statistical adjustment (Eden and Widmann 2014). WGs, on the other hand, are stochastic models that generate synthetic time series of local weather variables from parameterizations calibrated on historical observations (Wilks and Wilby 1999). In climate change applications, these parameters are then perturbed using GCM-simulated changes, enabling the WGs to incorporate the large-scale climate signal into the locally generated sequences. Although WGs are well established in the literature (see e.g. (Maraun et al. 2019; Tabari et al. 2021; Khazaei 2024)), they remain conceptually distinct from PP and MOS.

Within the PP framework, a wide range of methodologies has been developed, including traditional statistical techniques such as regression-based methods and analog methods, and more recently, advanced machine learning and deep learning approaches. Regression-based methods establish direct statistical relationships between large-scale atmospheric variables and local-scale climate variables, though they may struggle to capture non-linear dependencies and extreme events (Huang et al. 2011; Șan et al. 2023). Analog methods offer an alternative non-parametric strategy based on the assumption that similar large-scale atmospheric conditions produce similar local weather. They identify historical large-scale atmospheric states that most closely resemble a given GCM-simulated pattern and use the associated observed local-scale conditions as the downscaled estimate (Zorita and Von Storch 1999; Tian and Martinez 2012; Araya-Osses et al. 2020). Machine learning (ML) has significantly advanced statistical downscaling by offering powerful tools to capture complex, non-linear relationships between large-scale predictors and local-scale predictands. Deep learning (DL) has gained prominence in statistical downscaling (Sun et al. 2024) and Convolutional Neural Networks (CNNs) are especially well suited for this task, as they learn hierarchical spatial features and complex non-linear relationships from large datasets, making them highly suitable for enhancing the spatial resolution of climate model data (LeCun et al. 2015). CNN-based approaches have been successfully applied to downscale various climate variables, demonstrating their ability to capture complex spatial structures and relationships within climate fields (Serifi et al. 2021; Rampal et al. 2022; Lin et al. 2023; Soares et al. 2024). Baño-Medina et al. (2020, 2022) conducted a comprehensive assessment of multiple CNN architectures for downscaling temperature and precipitation over Europe under a PP framework, comparing them against traditional methods and highlighting their potential. PP techniques can achieve strong predictive skill; however, they are highly sensitive to the selection and quality of predictors

https://doi.org/10.5194/essd-2026-337
Preprint. Discussion started: 28 July 2026
© Author(s) 2026. CC BY 4.0 License.

and rely on the assumption that the historical predictor–predictand relationships remain stationary under future climate conditions.

A key advantage of MOS approaches lies in their simplicity: unlike PP methods, they generally do not require the selection of multiple predictors or consideration of domain-specific atmospheric processes. Often, the model-simulated value of the target variable from the nearest grid cell is used directly as the sole predictor. Among MOS techniques, bias correction (BC) methods have become increasingly widespread in climate change applications due to their ease of implementation and their effectiveness in reducing systematic errors in both GCM and RCM outputs. To this aim, BC methods adjust the statistical characteristics of model outputs to better match those of the observed climatology. Several BC techniques are available (Teutschbein and Seibert 2012; Maraun 2016; Menapace et al. 2025), ranging from simple linear adjustments to more sophisticated distribution-based methods. Linear scaling, one of the simplest methods, adjusts only the mean of the simulated data to match the observed one. Although these simple methods help avoid introducing artificial trends or changes in future climate model projections, they do not correct for biases in higher-order moments. Quantile Mapping (QM) is a widely used and robust bias correction technique that aligns the full distribution of simulated data with that of observations (Noël et al. 2021) by mapping simulated quantiles to their observed counterparts. QM can be implemented empirically, using the empirical cumulative distribution functions of the datasets (Themeßl et al. 2012), or parametrically, by fitting theoretical probability distributions (Piani et al. 2010). In practice, QM is calibrated by comparing simulated and observed distributions over a historical period, and the resulting transfer function is subsequently applied to future simulations to correct their distribution. A well-known limitation of traditional QM is its tendency to alter the climate change signal projected by the climate model, as it forces the future distribution to conform to the historical observed distribution, potentially dampening or amplifying trends. Quantile Delta Mapping (QDM) is an advancement of the traditional QM method, specifically designed to preserve the model climate change signal (Cannon et al. 2015; Fauzi et al. 2020; Xavier et al. 2022). Instead of mapping future quantiles directly to observed historical ones, QDM applies the modeled quantile changes from the historical to the future period to the observed historical distribution, thus maintaining the model projected relative changes while correcting historical biases.

Recent methods have integrated DL techniques with BC to improve downscaling performance. Sharma et al. (2024) developed a CNN-based bias correction for Indian summer monsoon rainfall, while Fulton et al. (2023) applied unpaired image-to-image translation networks combined with quantile mapping to correct GCM outputs. Wang and Tian (2024) combined a super-resolution deep residual network with QDM to simultaneously downscale and bias-correct climate variables from CMIP6 models. Zhang et al. (2026) applied quantile mapping at the native GCM resolution, followed by a super-resolution CNN to spatially downscale daily climate data. Together, these efforts underscore the growing recognition of multi-stage approaches that leverage complementary strengths of DL and BC techniques to address the multifaceted challenges of producing high-resolution climate projections.

This work proposes a statistical downscaling approach developed for CMIP6 GCM precipitation and near-surface temperature over the extended Mediterranean region, within the framework of the OurMED PRIMA project (https://www.ourmed.eu/). The objective is the development of an open-access climate projection dataset, named CMIP6-MedPlus, to support interdisciplinary climate impact research. The dataset comprises daily precipitation and mean, minimum, and maximum temperature at a spatial resolution of 0.25°, covering the period 1985–2100 and derived from five CMIP6 Global Climate Models under two Shared Socioeconomic Pathways (SSP1-2.6 and SSP3-7.0). The Mediterranean basin is widely recognized

https://doi.org/10.5194/essd-2026-337
Preprint. Discussion started: 28 July 2026
© Author(s) 2026. CC BY 4.0 License.

as a climate change hotspot (Giorgi and Lionello 2008; Tuel and Eltahir 2020; Todaro et al. 2022), where warming and hydroclimatic extremes are expected to intensify in the coming decades (MedECC et al. 2020). It is characterized by complex topography, strong land-sea contrasts, and marked hydroclimatic variability. In this context, enhancing the spatial resolution and accuracy of precipitation and temperature projections is essential for reliable regional climate impact assessments. The proposed downscaling method follows a hybrid, two-phase framework. In the first phase, a CNN is adopted to enhance spatial resolution and effectively capture local topographic and climatic features (Zhang et al., 2026), a step referred to as the regridding phase. In the second phase, biases are corrected using QDM. ERA5, a state-of-the-art global atmospheric reanalysis (Hersbach et al. 2020), serves as the reference dataset in both phases. The resulting CNN-QDM framework offers a practical and scalable approach for generating regional, bias-corrected climate projections. The CMIP6-MedPlus dataset aims to support climate impact assessments, hydrological modeling, and adaptation planning, particularly in regions characterized by heterogeneous climatic conditions. The dataset is freely available through Zenodo (https://doi.org/10.5281/zenodo.17898529, Todaro et al., 2025).

2 Methods

2.1 Study area and data

Climate projections of daily precipitation and daily mean, maximum, and minimum temperature are downscaled over a spatial domain that extends beyond the Mediterranean region as defined in the First Mediterranean Assessment Report (MAR1) by the Mediterranean Experts on Climate and Environmental Change (MedECC et al. 2020). This enlarged domain, as depicted in Fig. 1, facilitates state-level analyses across the wider Mediterranean region. It spans 18.5°W–45.25°E in longitude and 18.5°N–53.25°N in latitude, covering southern and central Europe, North Africa, and portions of the Middle East relevant for cross-boundary hydroclimatic processes.

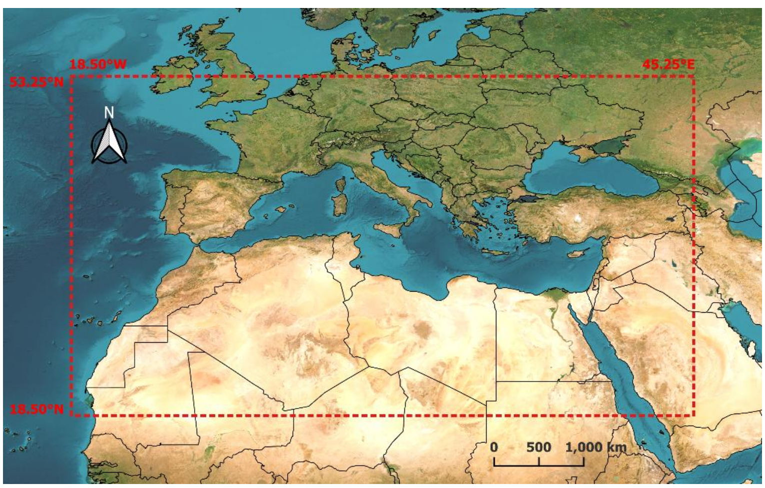

Figure 1. Study area covered by the dataset, indicated by the dashed red line.

The ERA5 reanalysis dataset (Hersbach et al. 2020) was used as reference. ERA5 provides hourly estimates of a wide range of atmospheric, land, and oceanic variables, with high temporal consistency and a spatial resolution of 0.25°, making it well suited for regional-scale climate applications.

https://doi.org/10.5194/essd-2026-337
Preprint. Discussion started: 28 July 2026
© Author(s) 2026. CC BY 4.0 License.

The climate across the extended Mediterranean region, exhibits marked spatial variability in both precipitation and temperature. Figure 2 shows the spatial distribution of annual precipitation and annual mean temperature over the 20-year period 1995–2014, based on ERA5 data. Annual precipitation is highest along the northern Mediterranean, particularly in orographically influenced areas such as the Alps, the Apennines, and the coastal ranges of Turkey and Greece, where totals exceed 1000–1500 mm per year. Precipitation decreases sharply toward the south, with much of North Africa receiving less than 150 mm annually, with some hyper-arid areas experiencing less than 1 mm. The annual mean temperature shows an inverse gradient, with cooler conditions in the northern Mediterranean, averaging around 10–15°C, and progressively warmer temperatures moving southward. The southern portion of the domain experiences mean temperatures exceeding 25°C. These patterns reflect the marked climatic diversity of the domain, ranging from Atlantic and continental climates in the northern regions to Mediterranean conditions and arid desert climates farther south, driven by strong gradients in precipitation and temperature.

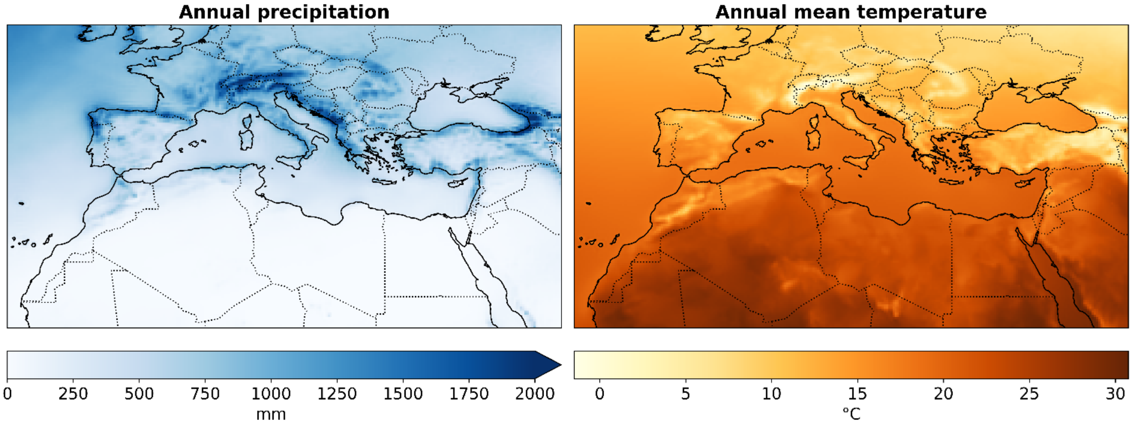

Figure 2. Annual precipitation and annual mean temperature over the study region for the period 1995–2014, derived from ERA5 data.

The downscaled dataset is based on simulations from five GCMs (Table 1) of the CMIP6 ensemble participating in the ScenarioMIP initiative (O'Neill et al. 2016). Model selection followed the recommendations of two official CORDEX documents: EURO-CORDEX CMIP6 GCM Selection & Ensemble Design: Best Practices and Recommendations (Sobolowski et al., 2023) and CORDEX Experiment Design and Archiving Specifications for Statistical Downscaling of CMIP6 (CORDEX, 2024). These documents identify priority GCMs for dynamical and statistical downscaling within the CMIP6 EURO-CORDEX framework and provide methodological guidance. The final set of models was chosen from this recommended pool guided by two criteria: (i) relatively high native global spatial resolution and (ii) the availability of the variables of interest. GFDL-ESM4, MPI-ESM1-2-HR, and MRI-ESM2-0 were selected from the CORDEX recommendations for statistical downscaling, based on their nominal resolution of approximately 100 km. NorESM2-MM and EC-Earth3-Veg were selected from the EURO-CORDEX recommendations, considering among the models with comparable resolution (100 km) those that provided all variables of interest. MPI-ESM1-2-HR appears in both sets of recommendations. The historical simulation period of the climate models covers 1985–2014, while future projections span 2015–2100.

https://doi.org/10.5194/essd-2026-337
Preprint. Discussion started: 28 July 2026
© Author(s) 2026. CC BY 4.0 License.

To capture a range of possible future conditions, two Shared Socioeconomic Pathways (SSPs; O'Neill et al. 2017) were considered in accordance with CORDEX guidelines and priorities: SSP1-2.6, reflecting a sustainable, low-emission pathway, and SSP3-7.0, representing a higher-emission pathway.

Table 1. CMIP6 GCMs selected for this study and their resolution.

Institute	Model	Grid resolution (Lon x Lat)
NCC	NorESM2-MM	1.25° x 0.94°
DKRZ	MPI-ESM1-2-HR	0.94° x 0.94°
EC-Earth-Consortium	EC-Earth3-Veg	0.70° x 0.70°
NOAA-GFDL	GFDL-ESM4	1.25° x 1.00°
MRI	MRI-ESM2-0	1.13° x 1.12°

2.2 Statistical downscaling

The proposed statistical downscaling approach follows a hybrid two-phase framework: (i) a Convolutional Neural Network (CNN) is used to increase the spatial resolution of climate model data (regridding phase), and (ii) a Quantile Delta Mapping (QDM) technique is applied to statistically adjust residual model biases while preserving the projected climate-change signal.

2.2.1 Data preprocessing

Prior to downscaling, to ensure consistency across the selected CMIP6 GCMs, all model outputs were interpolated to a common 1° grid using xESMF, a Python package for conservative remapping (Jiawei Zhuang et al. 2024). The ERA5 reanalysis dataset at 0.25° resolution served as the observational reference for all subsequent evaluations. For CNN training, ERA5 data were first upscaled to 1° to emulate the coarse structure of GCM predictors. These coarse ERA5 fields provided the CNN inputs, while the original 0.25° ERA5 data served as targets. This configuration allowed the network to learn a mapping from low- to high-resolution conditions while preserving spatial patterns.

2.2.2 Regridding via CNN

Convolutional Neural Networks (CNNs), widely used for extracting spatial patterns from images (LeCun et al. 2015), were employed to increase the spatial resolution of GCM outputs. In this framework, each "image" corresponds to the spatial distribution of a given climate variable for a single day over the study domain, and each day is processed independently, without exploiting temporal dependencies. Separate CNNs were trained for each climate variable. For temperature, three CNNs were used: one for daily mean temperature (T_{mean}), and two for the deviations of maximum ($\Delta T_{max} = T_{max} - T_{mean}$) and minimum ($\Delta T_{min} = T_{mean} - T_{min}$) temperature from the mean. This approach, by constraining the deviations to be positive, ensures physical consistency, enforcing $T_{max} \geq T_{mean} \geq T_{min}$ at every grid cell.

https://doi.org/10.5194/essd-2026-337
Preprint. Discussion started: 28 July 2026
© Author(s) 2026. CC BY 4.0 License.

Figure 3 illustrates the adopted CNN architecture. The network begins with two convolutional layers using ELU (Exponential Linear Unit) activation and "same" padding to preserve the spatial dimensions of the input feature maps, ensuring that important spatial information is not lost prematurely. These layers extract hierarchical spatial features from the low-resolution inputs. A dense layer with 3000 neurons then integrates the extracted spatial features into a unified representation capable of capturing complex and non-linear spatial relationships. During training, a dropout layer is applied to prevent overfitting by randomly deactivating a fraction of neurons, forcing the network to learn robust, generalized features. The output layer then generates high-resolution downscaled fields at the target 0.25° resolution. A conservative constraint layer (Harder et al. 2023; Fallah et al. 2023) is appended to enforce the preservation of coarse-scale quantities during downscaling. Because climate model data represent values as averages over each grid cell, this constraint ensures that the regridding process remains conservative, accurately redistributing coarse-grid quantities to the fine grid while maintaining physical consistency.

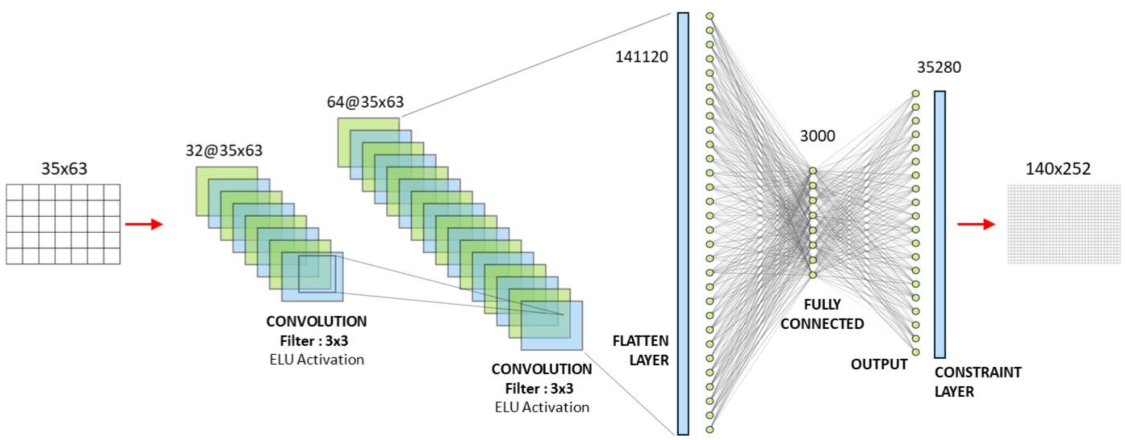

Figure 3. CNN architecture.

Let the low-resolution input be denoted by $\boldsymbol{X} \in \mathbb{R}^{H \times W}$, where H and W are the coarse spatial dimensions. The goal of the CNN is to generate a high-resolution field $\boldsymbol{Y} \in \mathbb{R}^{(NH)\times(NW)}$, where N is the spatial upscaling factor. In this study, H=35, W=63 and N=4. Each coarse-grid value x is associated with an $N \times N$ high-resolution patch, also called a super-pixel, consisting of $n = N^2$ values $\{y_i\}_{i=1}^{n}$. Conservation requires that the mean of these n downscaled values equals the original coarse input x. Depending on the variable, two different formulations of the constraint layer were applied. For mean temperature, an additive formulation enforce conservation while allowing both positive and negative deviations from the mean. Given the intermediate network outputs $\tilde{y}_j$, the final predictions (y_j) were computed as:

$$y_j = \tilde{y}_j + x - \frac{1}{n}\sum_{i=1}^{n} \tilde{y}_i\,, \quad j = 1, \ldots, n \tag{1}$$

For precipitation and for temperature deviations (ΔT_{max} and ΔT_{min}), where values must remain non-negative, a multiplicative constraint with a square transformation was employed. This guarantees both conservation and positivity:

https://doi.org/10.5194/essd-2026-337
Preprint. Discussion started: 28 July 2026
© Author(s) 2026. CC BY 4.0 License.

$$y_j = \tilde{y}_j{}^2 \cdot \frac{x}{\frac{1}{n}\sum_{i=1}^{n} \tilde{y}_i{}^2}, \quad j = 1, \dots, n \tag{2}$$

The CNNs were trained using the Adam optimizer (Kingma and Ba 2014) with mean squared error (MSE) as the loss function. Learning and dropout rates were tuned separately for precipitation and temperature to reflect their distinct spatial characteristics. For precipitation, a learning rate of 0.001 and a dropout rate of 0.5 were selected. The higher learning rate helps the network to capture localized extremes typical of precipitation fields, while a higher dropout rate mitigates overfitting. For temperature, the learning rate was reduced to 0.00001 and the dropout rate to 0.3. Because temperature fields are smoother and more spatially coherent, these settings promote stable training convergence and preserve fine-scale patterns without excessively suppressing the learned representations.

The CNNs were trained and validated on daily ERA5 data from 1970 to 2009 and tested on daily data from 2010 to 2023. Once trained, they were applied to GCM outputs to generate high-resolution projections at 0.25°.

2.2.3 Bias correction via QDM

After CNN-based regridding, the simulated data are aligned with the native spatial resolution of the ERA5 reference dataset. Then, bias correction was applied using Quantile Delta Mapping (QDM) independently at each grid cell. This method statistically adjusts the model outputs based on biases identified between observations (here ERA5 data) and simulated outputs (GCM outputs) over a common historical period, while preserving the relative changes projected by the models. QDM was applied separately for precipitation, mean temperature and the deviations of maximum and minimum temperature from the mean to ensure physically consistent downscaled projections.

Bias correction was performed on daily values, and empirical probability distributions were estimated on a monthly basis, using a three-month moving window (the target month plus the adjacent months) over the 30-year historical period 1985–2014. For example, January distributions were computed combining December, January, and February daily data to better capture inter-month correlations. Although traditional bias-correction methods typically use monthly windows, longer windows can offer a better balance between capturing seasonal extremes and limiting discontinuities at window edges (Pierce et al. 2015). For future projections (2015–2100), distributions were compute using a 30-year sliding window centered on the year of interest (Cannon et al. 2015; Tong et al. 2021); for instance, to correct January 2050, the period from 2035 to 2064 was considered, spanning 15 years before and after the target year. This dynamic window allows QDM to account for evolving distributions, capturing long-term changes in climate patterns.

For a given month, year and variable (e.g., temperature or precipitation), let $F_{obs,h}$ denote the empirical cumulative distribution function of observations (*obs*) for the historical period (*h*), and $F_{mod,h}$ and $F_{mod,p}$ the empirical distributions of the modelled values (*mod*) in the historical (*h*) and projected period (*p*), respectively. Given a model value in the projected period, $x_{mod,p}(t)$ at time t, its non-exceedance probability is defined as:

$$q(t) = F_{mod,p}\left(x_{mod,p}(t)\right) \tag{3}$$

A first quantile-mapping step aligns this value with the observed historical distribution:

$$\bar{x}(t) = F^{-1}_{obs,h}(q(t)) \tag{4}$$

where F^{-1}_{obs} is the inverse of the empirical distribution of observations.

Then, QDM estimates the model-projected quantile change by comparing the model projected and historical quantiles at the same probability level. Let $F^{-1}_{mod,p}$ and $F^{-1}_{mod,h}$ be the inverse of the empirical distribution of the model output for projected and historical period, respectively. The quantile change is expresses either additively, applied to mean temperature, or multiplicatively, applied to precipitation and temperature deviations, as follows:

$$\Delta(t) = F^{-1}_{mod,p}(q(t)) - F^{-1}_{mod,h}(q(t)) \tag{5}$$

$$\Delta(t) = \frac{F^{-1}_{mod,p}(q(t))}{F^{-1}_{mod,h}(q(t))} \tag{6}$$

This relative change is then applied to the corrected value of Eq. (4) in either the additive or multiplicative form:

$$\hat{x}(t) = \bar{x}(t) + \Delta(t) \tag{7}$$

$$\hat{x}(t) = \bar{x}(t) \cdot \Delta(t) \tag{8}$$

When correcting the model outputs in the historical period $F_{mod,p} = F_{mod,h}$, and the correction reduces to the standard quantile mapping of Eq. (4).

2.3 Evaluation methods

The evaluation of the downscaling framework was conducted in two stages: first, assessing the CNN-based regridding alone, and second, evaluating the full downscaling output after the application of QDM bias correction.

In the first stage, the CNN was evaluated solely on its regridding capability, using coarse- and fine-resolution representations of the reference dataset (ERA5). Specifically, the high-resolution outputs produced by the CNN were compared with the original high-resolution ERA5 fields. Since both datasets are temporally aligned, performance was assessed through pairwise daily comparisons over the test period 2010–2023 (5113 maps), using root mean square error (RMSE) as the metric. In addition, the results were then compared with those obtained using a conventional nearest-neighbor regridding approach, which assigns to each high-resolution grid cell the value of the closest low-resolution grid cell.

In the second stage, the full downscaling process (CNN + QDM) was evaluated with a different rationale, as its goal is not to replicate individual daily values but to adjust the statistical distribution of simulated data while preserving projected climate change signals. The evaluation therefore focused on long-term statistical properties. The selected metrics (Table 2) are a subset of those proposed by the VALUE validation framework (Maraun et al. 2015), ensuring methodological consistency and comparability with previous studies. Downscaling performance was assessed over the reference historical period 1995–2014. For each climate model and each grid cell, both the raw GCM outputs interpolated to 0.25° using nearest-neighbor mapping and the fully downscaled fields produced after CNN regridding and QDM bias correction were compared with the

https://doi.org/10.5194/essd-2026-337
Preprint. Discussion started: 28 July 2026
© Author(s) 2026. CC BY 4.0 License.

reference dataset ERA5. The analysis includes the bias in the daily mean, in the 2nd percentile (P2) and the 98th percentile (P98) of daily distributions, as well as in a set of extreme indicators describing prolonged warm, cold, wet, and dry conditions: the Warm Annual Maximum Spell (WAMS), Cold Annual Maximum Spell (CAMS,), Wet Annual Maximum Spell (WetAMS), and Dry Annual Maximum Spell (DryAMS). For each indicator, the bias was calculated as the difference between the model estimates and the reference values. The computation of each indicator is summarized as follows:

- Mean bias: computed by deriving the daily climatological mean over the 1995–2014 period for both the model and the ERA5 reference datasets, and then taking the difference between the two.
- P2 and P98 biases: estimated by calculating, for each year, the 2nd and 98th percentiles of daily values for both datasets, followed by the mean of the annual percentile values over the 1995–2014 period. The bias was then obtained as the difference between the model and reference multi-year averages.
- WAMS and CAMS: the WAMS is defined as the longest sequence of consecutive days within a year when the daily mean temperature exceeds the 90th percentile of the reference climatology, while the CAMS corresponds to the longest sequence of consecutive days when the daily mean temperature falls below the 10th percentile. For both indicators, the median of the annual values over the 1995–2014 period was computed for the model and the reference datasets, and their difference was used to quantify the bias.
- WetAMS and DryAMS: the WetAMS represents the longest sequence of consecutive wet days (precipitation ≥ 1 mm/day) in a year, whereas the DryAMS represents the longest sequence of consecutive dry days (precipitation < 1 mm/day). As for the temperature-based indicators, the median of the annual values over the 1995–2014 period was used for comparison between the model and the reference datasets.

Table 2. Summary of the metrics used to assess the performance of QDM during the reference period 1995–2014. Each metric represents the bias between model and reference datasets for mean (Tm), minimum (Tn) and maximum (Tx) temperature, and precipitation (Pr) variables.

Metric	Description	Variable(s)	Units
Mean bias	Bias in daily climatological mean	$T_{min}, T_{mean}, T_{max}$ Pr	°C, %
P2 bias	Bias in 2nd percentile	$T_{min}, T_{mean}, T_{max}$	°C
P98 bias	Bias in 98nd percentile	$T_{min}, T_{mean}, T_{max}$ Pr	°C, %
WAMS bias	Bias in Warm Annual Maximum Spell	$T_{min}, T_{mean}, T_{max}$	days
CAMS bias	Bias in Cold Annual Maximum Spell	$T_{min}, T_{mean}, T_{max}$	days
WetAMS bias	Bias in Wet Annual Maximum Spell	Pr	days
DryAMS bias	Bias in Dry Annual Maximum Spell	Pr	days

https://doi.org/10.5194/essd-2026-337
Preprint. Discussion started: 28 July 2026
© Author(s) 2026. CC BY 4.0 License.

3 Results

3.1 Data records

The CMIP6-MedPlus dataset provides statistically downscaled daily projections of precipitation and near-surface air temperature over an extended Mediterranean domain for the period 1985–2100. The dataset includes daily precipitation and daily mean, maximum and minimum temperature, derived from an ensemble of five CMIP6 GCMs under the two scenarios SSP1-2.6 and SSP3-7.0.

All data are distributed in NetCDF4 format, with a total volume of approximately 200 GB. Each NetCDF file contains downscaled projections for a single climate variable from one GCM and covers both the historical period (1985–2014) and the future projection period (2015–2100). The data are provided on a regular latitude–longitude grid at 0.25° spatial resolution. Each file includes latitude and longitude bounds, as well as separate time coordinates for historical and scenario periods. An overview of the main characteristics of the CMIP6-MedPlus dataset is provided in Table 3.

Table 3. Summary of the main features of the CMIP6-MedPlus dataset

Dataset title	CMIP6-MedPlus
Dataset type	Gridded
Dimensions	time, longitude, latitude
Data format	NetCDF4
Temporal coverage	Historical period: 1985–2014; Scenario period: 2015–2100
Temporal resolution	Daily
Spatial extent	Longitude: −18.5 to 45.25 degrees east; Latitude: 18.5 to 53.25 degrees north
Coordinate system	WGS84 (EPSG:4326)
Spatial resolution	0.25°
Climate variables Long name – short name – [units]	Total precipitation amount – pr – [mm]; 2 m temperature – tas – [°C]; 2 m maximum temperature – tasmax – [°C]; 2 m minimum temperature – tasmin – [°C];
Climate models	EC-Earth3-Veg GFDL-ESM4 MPI-ESM1-2-HR MRI-ESM2-0 NorESM2-MM
Scenarios	SSP1-2.6 and SSP3-7.0

https://doi.org/10.5194/essd-2026-337
Preprint. Discussion started: 28 July 2026
© Author(s) 2026. CC BY 4.0 License.

3.1.1 Usage notes

The CMIP6-MedPlus dataset is designed to support climate impact assessments at the Mediterranean and sub-regional scales by providing projections of precipitation and temperature across a broad domain. The 0.25° spatial resolution is suitable for applications focusing on large-scale hydrological responses, regional climate risk assessments, and sectoral impact analyses at regional, or transnational scales.

To account for uncertainty inherent in climate projections, users are encouraged to conduct impact simulations separately for each of the five CMIP6 GCMs included in the dataset and to analyze the resulting spread of outcomes. Simulations should also be performed under both SSP1-2.6 and SSP3-7.0 scenarios, representing low and high challenges to mitigation, respectively, in order to explore a range of plausible future climate conditions.

For local or site-specific impact assessment studies, however, the 0.25° resolution may be insufficient to fully capture fine-scale climatic variability, particularly in areas characterized by complex topography, strong land–sea contrasts, or pronounced local gradients. In these cases, it is advisable to apply an additional statistical adjustment step using CMIP6-MedPlus as a baseline and locally observed data from gauging stations where available.

3.2 Performance evaluation

3.2.1 Performance of regridding via CNN

Figure 4 illustrates the RMSE maps for precipitation and temperature (mean, maximum and minimum), comparing the performance of the CNN-based regridding against the nearest-neighbor (NN) method over the test period 2010–2023. Across all variables, the CNN achieves substantially lower RMSE values than the NN. The NN results (top row) exhibit pronounced grid-pattern artifacts, particularly over complex terrain such as the Alps, the Apennines, and coastal areas, reflecting discontinuities introduced by the coarse grid sampling. In contrast, the CNN-based results (bottom row) display a marked reduction in RMSE, indicating improved consistency and spatial coherence of the regridded fields. For precipitation, improvements are especially notable in mountainous and coastal areas, where local variability is better captured by the CNN. The domain-mean RMSE is comparable between the NN and CNN methods, at around 0.6 mm, but maximum errors differ markedly: 9.8 mm for NN and values below 4.2 mm for CNN.

For temperature, the CNN consistently outperforms NN across the entire domain. For mean temperature, the domain-averaged RMSE is 0.58 °C for NN and 0.20 °C for CNN, with maximum errors of 9.0 °C and below 1.0 °C, respectively. For minimum temperature, the NN has a mean RMSE from 0.71 °C compared to 0.38 °C of the CNN and the maximum error from over 10 °C goes below 1.6 °C. Similarly, for maximum temperature, the mean RMSE decreases from 0.70 °C for NN to 0.27 °C for CNN, and the maximum error drops from values above 8 °C to below 1.2 °C.

These results demonstrate that the CNN model effectively learns complex spatial relationships between coarse and fine-scale fields, outperforming traditional nearest-neighbor interpolation. This improved accuracy provides a more consistent starting point for the subsequent bias correction stage, enabling point-by-point adjustments that better reflect local climatological patterns.

https://doi.org/10.5194/essd-2026-337
Preprint. Discussion started: 28 July 2026
© Author(s) 2026. CC BY 4.0 License.

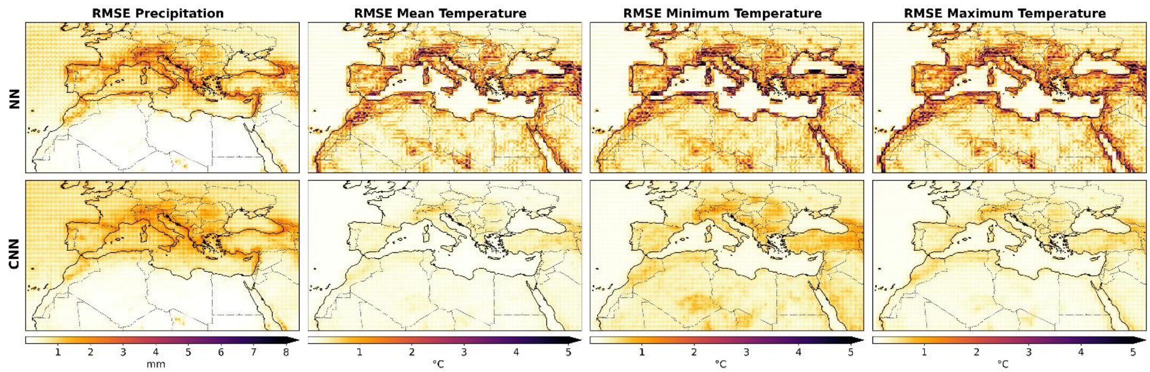

Figure 4. Comparison of the spatial distribution of RMSE for daily precipitation and temperature variables obtained with the nearest-neighbor (NN, top row) and CNN-based (bottom row) regridding approaches for the test period 2010–2023.

3.2.2 Performance of the full downscaling framework

The performance evaluation is carried out over the historical reference period 1995–2014 by comparing the fully downscaled outputs with the ERA5 reference dataset and, for context, with the raw GCM outputs (interpolated to 0.25° via nearest-neighbor mapping). To illustrate inter-model differences, the mean bias of annual precipitation and annual mean, maximum and minimum temperature is shown separately for each GCM over the study domain. The maps in Fig. 5 show the mean bias of annual precipitation, expressed as the percentage difference between GCM and ERA5 data. In the raw simulations, the models exhibit large and spatially heterogeneous biases, with substantial inter-model variability. In the southern portion of the domain, biases frequently exceed ±90%; however, it is important to note that these large relative errors are associated with regions characterized by very low annual precipitation, where even small absolute deviations result in high percentage biases. Negative biases dominate in several areas of Southern Europe in EC-Earth3-Veg, NorESM2-MM, and MPI-ESM1-2-HR, whereas overestimation prevail across much of Europe in MRI-ESM2-0 and GFDL-ESM4. After applying the downscaling procedure, these biases are substantially reduced, with values approaching zero over most of the domain.

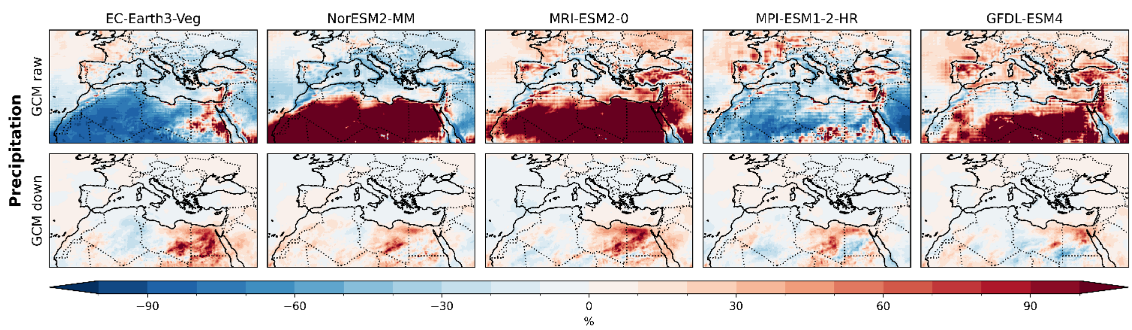

Figure 5. Mean bias of annual precipitation (in %, relative to the ERA5) for five GCMs in the period 1995–2014. The top row shows the raw model outputs, while the bottom row shows the corresponding downscaled simulations.

Figure 6 presents the spatial distribution of temperature biases. In the raw simulations, GCMs exhibit large biases, with notable inter-model differences. EC-Earth3-Veg and GFDL-ESM4 predominantly underestimate mean, minimum and maximum temperature across the study area, whereas NorESM2-MM underestimates in the southern portion of the domain and overestimates in the north. MRI-ESM2-0 presents mix of under- and overestimations, with a predominant overestimation of

https://doi.org/10.5194/essd-2026-337
Preprint. Discussion started: 28 July 2026
© Author(s) 2026. CC BY 4.0 License.

minimum temperature. For MPI-ESM1-2-HR, mean temperature shows both under- and overestimations, while minimum temperature is predominantly overestimated and maximum temperature underestimated, resulting in a substantial negative bias in the diurnal temperature range. Following the application of the downscaling procedure, these biases are markedly reduced, with values approaching zero over the entire region. This highlights the effectiveness of the downscaling method in mitigating systematic temperature biases and enhancing the reliability of GCM outputs.

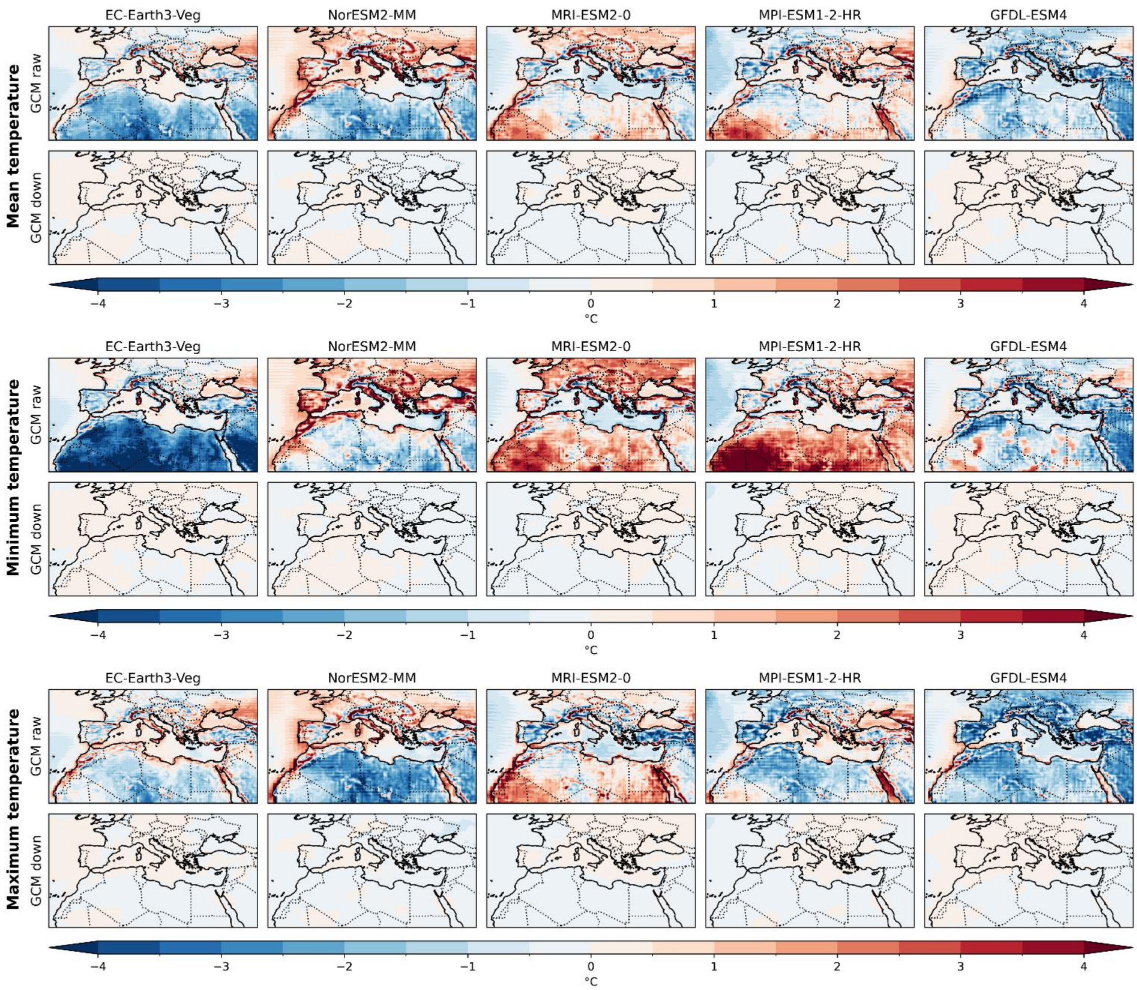

Figure 6. Mean bias of mean (top), minimum (middle) and maximum (bottom) temperature (in °C, relative to the ERA5) for five GCMs in the period 1995–2014. The top row of each sub-plot shows the raw model outputs, while the bottom row shows the corresponding downscaled simulations.

Figure 7 presents the precipitation bias for different metrics, based on the ensemble mean of the five GCMs. For the raw simulations, both the mean bias and the P98 bias (98th percentile of daily precipitation) reveal widespread and substantial errors, with particularly strong overestimations across the southern portion of the domain. After downscaling, these systematic errors are greatly reduced, and most areas display values close to zero, indicating a substantial correction of both mean and extreme precipitation. The Wet Annual Maximum Spell (WetAMS) bias in the raw GCMs points to an overestimation of wet

https://doi.org/10.5194/essd-2026-337
Preprint. Discussion started: 28 July 2026
© Author(s) 2026. CC BY 4.0 License.

spell persistence in several regions, especially over western and northern Europe. Downscaling largely removes these discrepancies, leaving only localized residual biases of minor magnitude. Likewise, the Dry Annual Maximum Spell (DryAMS) bias highlights pronounced errors in the raw simulations, with significant underestimation of dry spell duration across Northeast Africa and an overestimation in Northwestern Africa and the eastern Mediterranean coasts. These biases are strongly attenuated in the downscaled results across the domain.

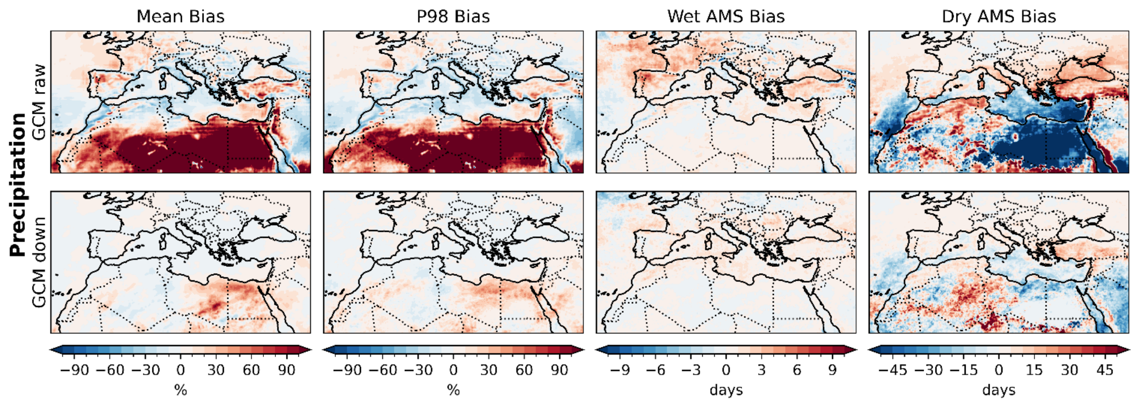

Figure 7. Annual precipitation mean bias, 98th percentile (P98) of daily precipitation bias, Wet Annual Maximum Spell (WetAMS) bias, and Dry Annual Maximum Spell (DryAMS) bias based on the ensemble mean of five GCM outputs for the period 1995–2014. The top row shows the raw model outputs, while the bottom row shows the corresponding downscaled simulations. Biases are all relative to ERA5.

Figure 8 presents temperature biases for mean, minimum, and maximum daily temperature, as well as for extreme and persistence-based indicators, based on the ensemble mean of the five GCMs. In the raw simulations, systematic biases are evident across the domain. From the mean bias maps, temperatures exhibit widespread biases, with a predominant underestimation in maximum temperature and over North Africa and the eastern Mediterranean. These patterns are also evident in the percentile-based metrics, with the P2 and P98 biases showing marked deviations: the P2 bias (2nd percentile, reflecting cold extremes) resembles the mean pattern but with larger magnitudes, while the P98 bias highlights pronounced overestimations, particularly along the coasts, and underestimations of maximum temperature over northern Europe.

Persistence indicators are similarly affected. The WAMS bias (Warm Annual Maximum Spell) in the raw GCMs indicates a predominant overestimation of warm spell duration, while the CAMS bias (Cold Annual Maximum Spell) shows a consistent underestimation of cold spells across central and eastern Europe, alongside an overestimation over northern Africa and the Middle East.

After applying downscaling, systematic errors are substantially reduced across all metrics. Biases in mean temperature, as well as in P2 and P98, converge toward near-zero values throughout most of the domain, with only localized residual deviations. Persistence metrics also improve markedly: the strong WAMS and CAMS biases in the raw GCMs are largely removed, leaving only minor deviations. Overall, the downscaled results demonstrate a strong capacity to correct both mean-state and extreme temperature biases, including those related to the persistence of warm and cold spells.

https://doi.org/10.5194/essd-2026-337
Preprint. Discussion started: 28 July 2026
© Author(s) 2026. CC BY 4.0 License.

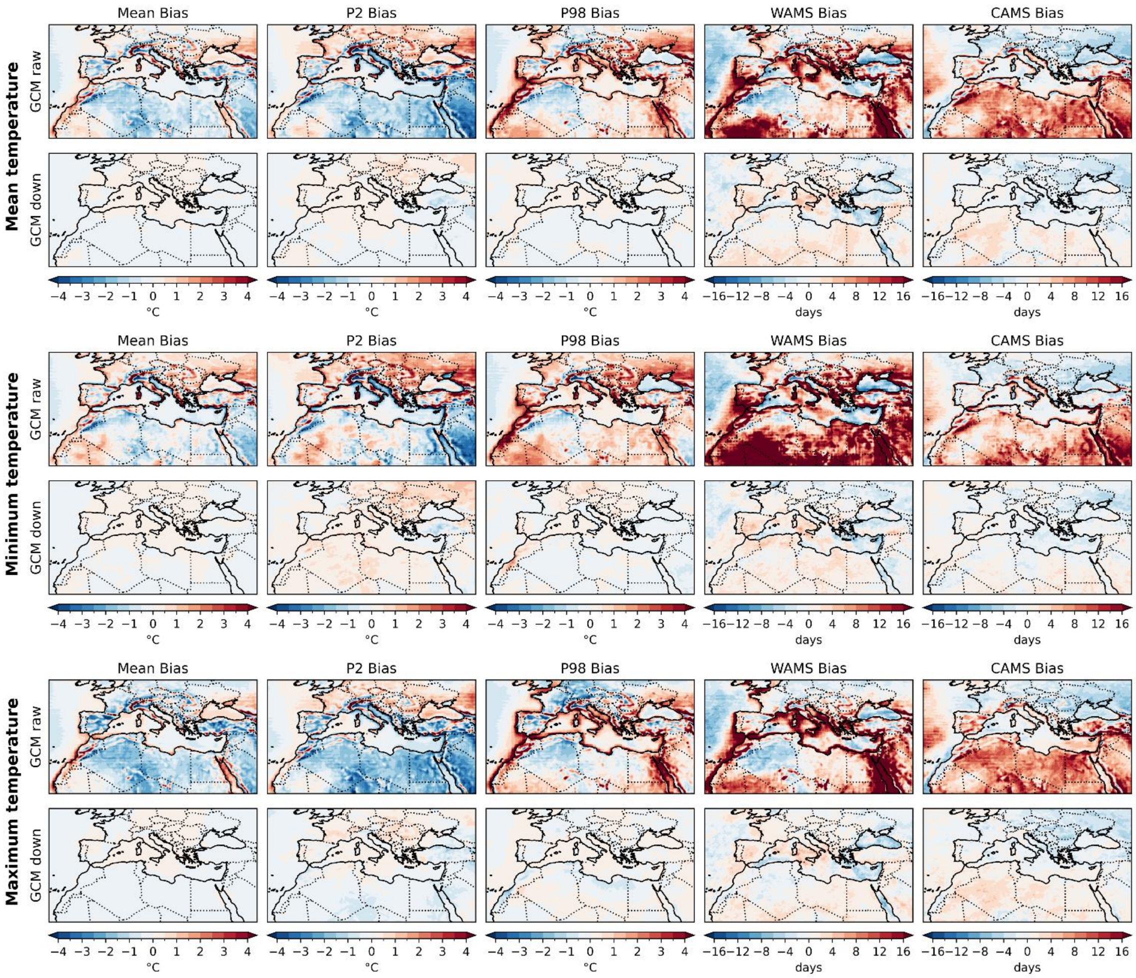

Figure 8. Mean, minimum and maximum temperature mean bias, 98th percentile (P98) of temperature bias, Warm Annual Maximum Spell (WAMS) bias, and Cold Annual Maximum Spell (CAMS) bias based on the ensemble mean of five GCM outputs for the period 1995–2014. The top row of each sub-panel shows the raw model outputs, while the bottom row shows the corresponding downscaled simulations. Biases are all relative to ERA5.

3.2.3 Added value of applying CNN before QDM

The results presented in the previous section demonstrate that the full downscaling framework effectively reduces both mean and distribution-based biases over the reference period. However, these diagnostics alone do not fully capture the added value of performing the CNN-based spatial refinement before bias correction. This is because QDM is designed to adjust the local statistical distribution of a variable and is therefore highly effective at reducing biases in metrics derived from long-term distributions, such as mean values and percentiles. Consequently, when performance is assessed using time-aggregated statistics over the historical period, different regridding strategies followed by QDM may lead to similarly satisfactory results. The main added value of the CNN lies in its ability to reconstruct the spatial structure of daily fields. Unlike nearest-neighbor remapping, which merely transfers coarse-scale information onto the target grid and retains block-like, spatially simplified

https://doi.org/10.5194/essd-2026-337
Preprint. Discussion started: 28 July 2026
© Author(s) 2026. CC BY 4.0 License.

patterns, the CNN generates spatially refined fields that are more coherent with the fine-scale structure of the observational reference.

However, this added value cannot be assessed through a deterministic day-by-day comparison with observations. Because model outputs and observations are not temporally synchronized, the same calendar day in the model does not correspond to the same realized weather event. Pointwise daily error metrics are therefore not meaningful in this context. Instead, the CNN contribution should be evaluated in terms of the spatial realism and effective spatial resolution of the generated daily fields. Figure 9 illustrates this aspect through an example of a daily precipitation field, with a zoom over Italy. The NN+QDM result retains the block-like features inherited from the coarse-resolution model field, whereas the CNN+QDM map exhibits a smoother and more spatially coherent structure, with transitions and localized features that better reflect the expected fine-scale variability. The figure thus makes clear that the added value of the CNN is not primarily reflected in aggregated statistical metrics after QDM, but in the improved spatial realism of individual daily fields.

This effect is especially evident for precipitation, owing to its strong small-scale variability and intermittency. Since QDM operates independently at each grid cell, it adjusts the local distribution but does not reconstruct spatial coherence across neighboring cells. As a consequence, the coarse-grid imprint remains visible when the input field is obtained by nearest-neighbor remapping, whereas the CNN helps reduce this artefact. The benefit of applying CNN before QDM should therefore be understood mainly in terms of improved spatial realism, rather than further gains in metrics that are already largely determined by QDM.

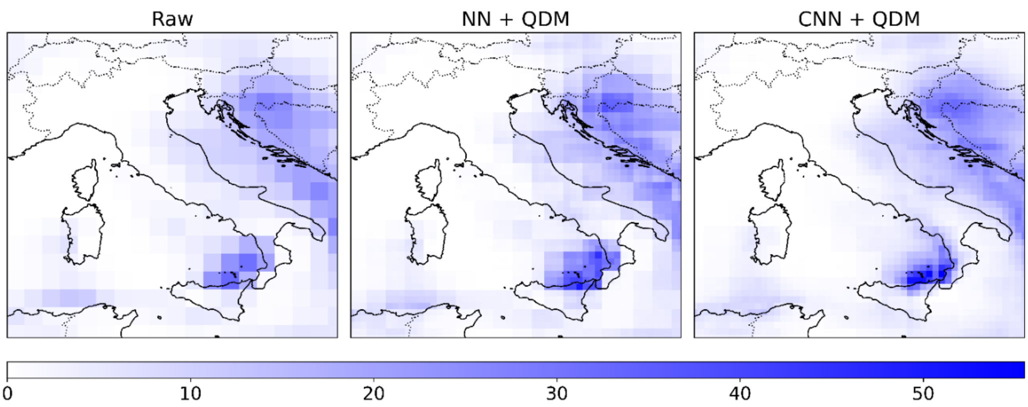

Figure 9. Zoom over Italy showing an example of a daily precipitation field (9 February 2065) for one GCM (EC-Earth3-Veg) and one scenario (SSP1-2.6), comparing the raw model output, the nearest-neighbor remapping followed by QDM (NN+QDM), and the CNN-based spatial refinement followed by QDM (CNN+QDM).

3.2.4 Future projections

Figure 10 and Figure 11 show the projected changes in annual precipitation and annual mean temperature, respectively, relative to the 1995–2014 reference period, based on the ensemble mean of the five downscaled CMIP6 climate models. Anomalies are shown for three future periods: short-term (ST, 2021–2040), medium-term (MD, 2041–2060), and long-term (LT, 2081–2100).

Projected changes in annual precipitation (Fig. 10) display a spatially heterogeneous pattern. Under SSP1-2.6, precipitation anomalies remain generally modest across the century. In the ST period, most of southern Europe and the western

https://doi.org/10.5194/essd-2026-337
Preprint. Discussion started: 28 July 2026
© Author(s) 2026. CC BY 4.0 License.

Mediterranean show changes within ±10%, while localized increases appear over the eastern Mediterranean and the Sahara–Sahel transition zone, where positive anomalies exceed +20 to +40%. These features persist in the MT period. By the LT period, SSP1-2.6 still shows relatively limited and spatially confined drying across the studied domain, although reductions become more evident over Morocco, Algeria, Tunisia, and Libya. Conversely, the positive anomalies south of the Sahara remain evident throughout the century. A portion of these pronounced positive or negative percentage anomalies, both in the Mediterranean and in the Sahara–Sahel region, reflects the fact that baseline precipitation amounts are very low in these areas; therefore, even small absolute changes translate into large relative changes, producing strong apparent increases or decreases in the maps. Under SSP3-7.0, the drying signal strengthens markedly with time. In the ST period, emerging reductions appear along the northern African coast and parts of the central Mediterranean. By the MT period, a more coherent drying band is established across southern Europe, with intensifying deficits over western North Africa. In the LT period, precipitation declines become more widespread across nearly the entire domain, with reductions exceeding -20 to -30% over large portions of North Africa. Increases south of the Sahara persist across all periods, consistent with the mechanisms already noted for this region.

Temperature projections (Fig. 11) indicate a robust and spatially coherent warming across the entire domain under both SSP1-2.6 and SSP3-7.0. Under SSP1-2.6, warming remain moderate throughout the century. In the ST period, temperature anomalies generally range between +0.5 and +1.5 °C across most of the domain. By the MT period, warming becomes slightly more widespread, with increases of similar magnitude. In the LT period, SSP1-2.6 shows a clear stabilization, with long-term anomalies remaining mostly below +1.5 °C (except for a few very localized areas approaching +2 °C), and even slight cooling emerging over parts of the northwestern domain. In contrast, under SSP3-7.0, the warming signal intensifies substantially with time. In the ST period, temperature increases remain below +1.5 °C across the entire domain. By the MT period, warming becomes more pronounced, reaching around +2 °C over southern Europe and North Africa, with some localized areas approaching +2.5 °C. In the LT period, the warming intensifies substantially and becomes spatially uniform, with anomalies commonly exceeding +4 °C across North Africa, the Middle East, and some parts of southern Europe.

https://doi.org/10.5194/essd-2026-337
Preprint. Discussion started: 28 July 2026
© Author(s) 2026. CC BY 4.0 License.

Open Access Earth System Science Data Discussions

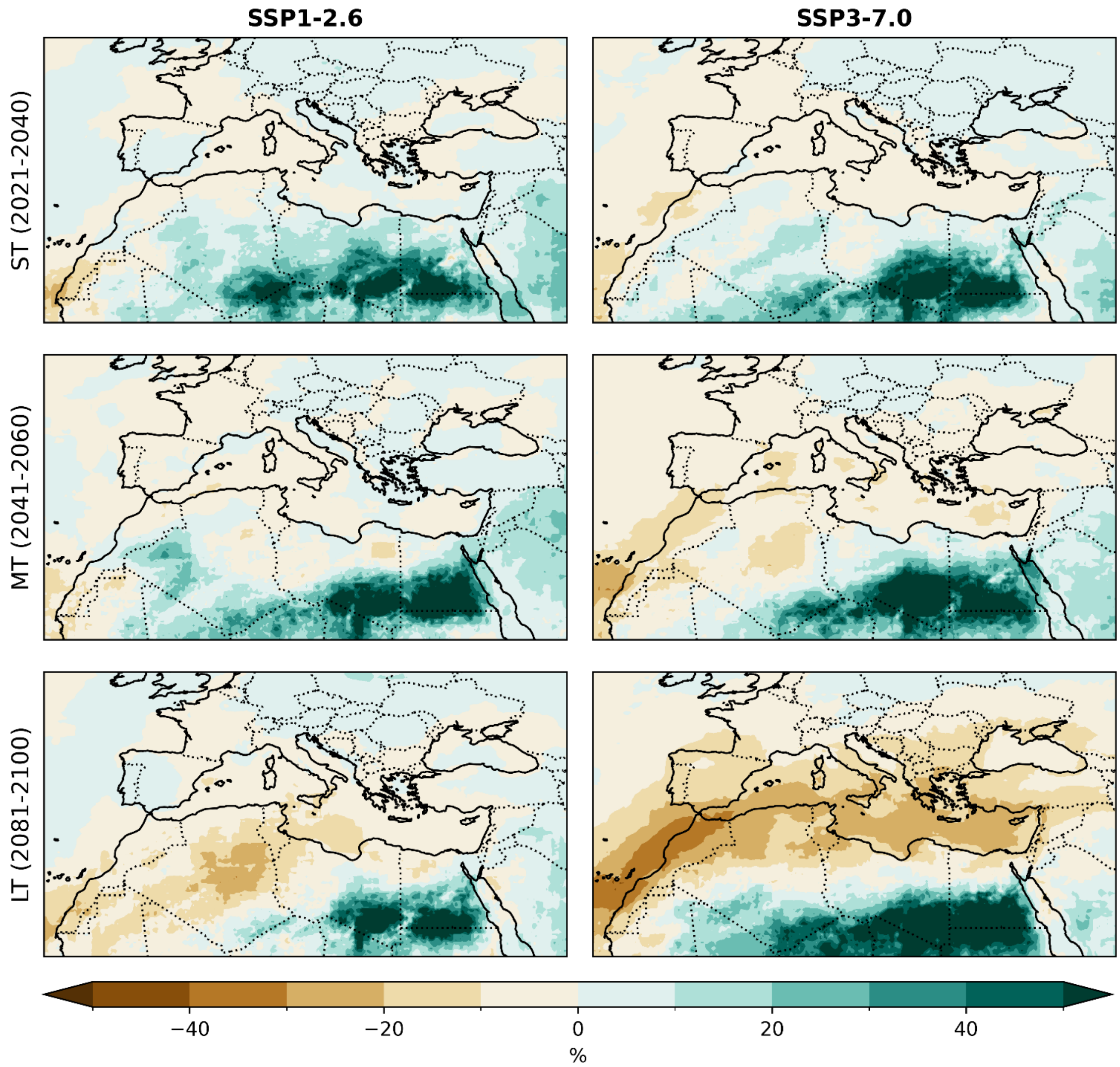

Figure 10. Projected percentage changes in total annual precipitation relative to the 1995–2014 reference period, based on the ensemble mean of the five climate models. Changes are shown for three future periods—short-term (ST; 2021–2040), medium-term (MT; 2041–2060), and long-term (LT; 2081–2100)—under two Shared Socioeconomic Pathways (SSP1-2.6 and SSP3-7.0).

https://doi.org/10.5194/essd-2026-337
Preprint. Discussion started: 28 July 2026
© Author(s) 2026. CC BY 4.0 License.

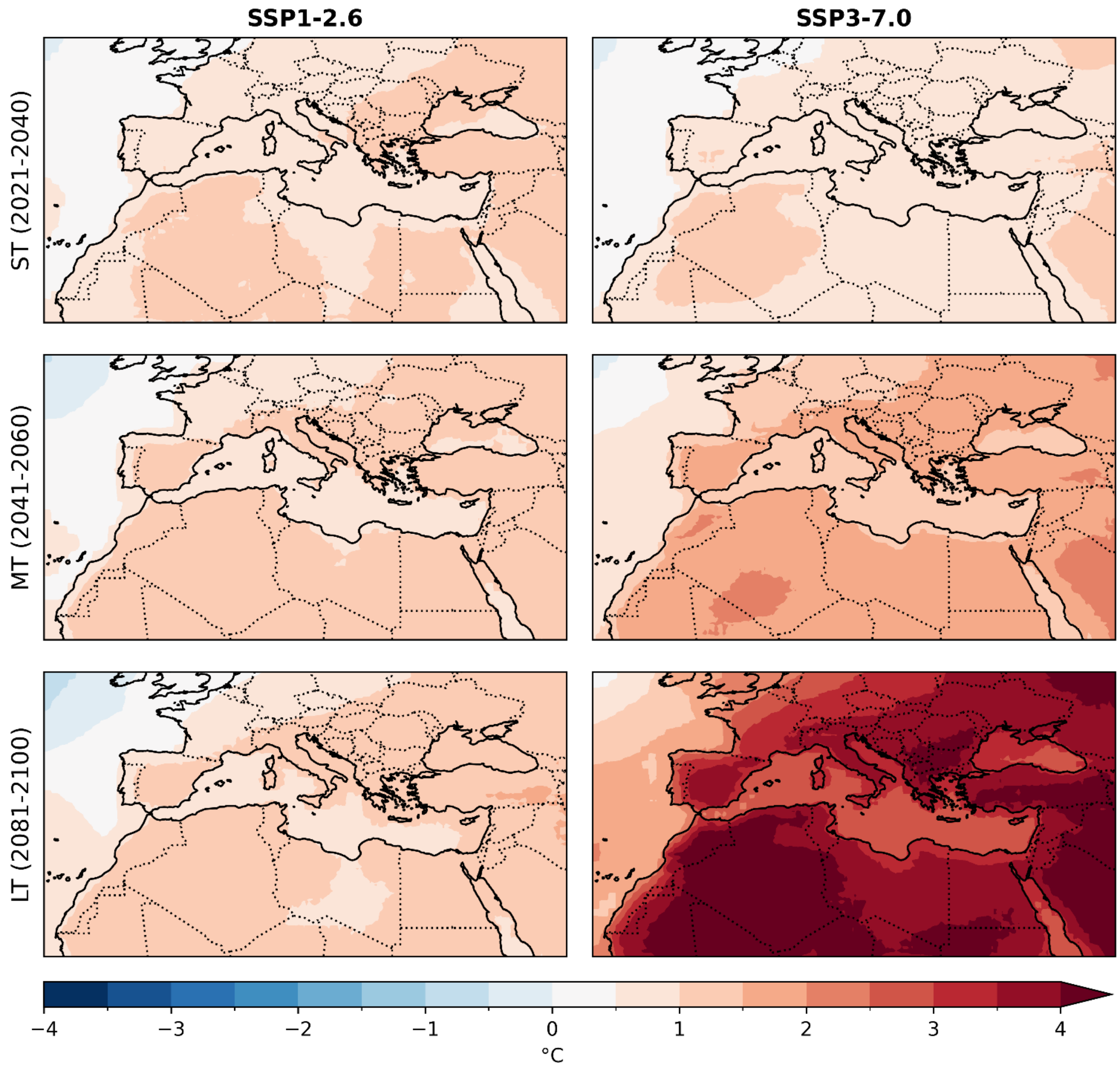

Figure 11. Projected changes in mean temperature relative to the 1995–2014 reference period, based on the ensemble mean of the five climate models. Changes are shown for three future periods—short-term (ST; 2021–2040), medium-term (MT; 2041–2060), and long-term (LT; 2081–2100)—under two Shared Socioeconomic Pathways (SSP1-2.6 and SSP3-7.0).

4 Discussion

This section discusses the main assumptions, and limitations of the proposed framework. As with any statistical downscaling framework, the proposed approach relies on assumptions that may introduce limitations. Statistical methods infer relationships between large-scale GCM fields and local climate information, with the aim of better representing local-scale variability and spatial detail. They are computationally efficient and scalable to large domains; however, they cannot introduce physical processes beyond those represented in the GCMs and rely on the assumption that empirical relationships derived from historical data remain valid under future climate conditions. Dynamical downscaling, by contrast, involves embedding

https://doi.org/10.5194/essd-2026-337
Preprint. Discussion started: 28 July 2026
© Author(s) 2026. CC BY 4.0 License.

regional climate models that explicitly simulate physical processes at finer scales, allowing for the emergence of phenomena such as local convection, orographic effects, and mesoscale circulations. This makes dynamical downscaling particularly advantageous in regions with complex terrain or where small-scale processes strongly influence climate patterns. However, dynamical approaches are computationally demanding and regional climate model outputs are not always available. In practice, statistical and dynamical downscaling are complementary, and statistical approaches remain a practical and efficient solution when climate information is needed at regional and sub-regional scales (Jacob et al. 2020).

Beyond these general considerations, additional sources of uncertainty arise from specific methodological choices adopted in the present framework. The CNN-based spatial refinement is inherently data-driven and sensitive to the quality and representativeness of the training data, which may limit its ability to generalize under non-stationary climate conditions. These challenges are particularly relevant for precipitation, whose intermittent and highly skewed distribution makes it difficult to accurately reproduce the intensity of localized extremes. Moreover, the inclusion of a conservative constraint layer to ensure physical consistency between regridded fields and coarse-scale inputs may introduce block-like spatial patterns in regions where precipitation structures are weakly defined. While this represents a deliberate trade-off, conservation is essential, particularly for precipitation. When precipitation patterns are weak, sparse, or poorly organized, the CNN may fail to recover a sufficiently informative fine-scale structure; under these conditions, the conservation constraint guarantees physical consistency between the downscaled field and the original coarse-scale input. Finally, it should be noted that the CNN enhances spatial detail but does not correct systematic model biases, which are addressed separately through bias correction.

Additional sources of uncertainty are associated with the subsequent bias-correction phase. QDM shares several limitations common to distribution-based correction methods, including the assumption that the bias structure identified during the historical period remains consistent in the future. Additionally, QDM can be sensitive in regions with very low precipitation and frequent zero-precipitation days, such as arid zones, where small absolute differences between modeled and reference quantiles may result in disproportionately large relative corrections if not carefully constrained. Moreover, QDM adjusts the marginal distribution of climate variables but does not explicitly correct temporal characteristics, such as wet–dry spell length or event persistence; consequently, biases in temporal autocorrelation or event clustering may persist after correction. The effectiveness of bias correction also depends on the quality and temporal extent of the reference dataset, and performance may degrade in regions with sparse or limited observations. Although ERA5 can compensate for missing observations through its modeling framework, its performance may degrade and become less reliable in areas with sparse or absent observations. Despite these limitations, QDM remains a widely used and robust method for adjusting systematic model errors while preserving the underlying climate change signal.

5 Conclusions

This study presents CMIP6-MedPlus, a statistically downscaled climate projection dataset for the extended Mediterranean region, developed from five CMIP6 GCMs under the SSP1-2.6 and SSP3-7.0 scenarios and including daily precipitation and daily minimum, mean, and maximum near-surface air temperature. The dataset is generated through a framework that combines a CNN-based spatial refinement step with a subsequent bias correction step via QDM, which adjusts local distributions while preserving the projected climate-change signal. The evaluation over the historical reference period shows that the framework substantially reduces systematic biases in precipitation and temperature across the study domain. In

https://doi.org/10.5194/essd-2026-337
Preprint. Discussion started: 28 July 2026
© Author(s) 2026. CC BY 4.0 License.

particular, the results show that QDM is effective in improving long-term distribution-based diagnostics, while the CNN primarily contributes to a more spatially coherent representation of daily fields.

CMIP6-MedPlus provides a consistent set of downscaled projections that can support a range of applications in climate-impact research, including hydrology, water resources, agriculture, ecosystem studies, and climate-risk assessment, and represents a baseline for subsequent refinement in basin-scale and local-scale applications.

Data Availability

The CMIP6 GCM data were accessed through the Earth System Grid Federation (ESGF) archive (https://esgf-node.llnl.gov/projects/cmip6/), while ERA5 reanalysis data were retrieved from the Copernicus Climate Data Store (CDS, https://cds.climate.copernicus.eu/datasets/reanalysis-era5-single-levels?tab=overview).

The CMIP6-MedPlus dataset generated in this study is publicly available through the Zenodo repository (https://doi.org/10.5281/zenodo.17898529, Todaro et al., 2025).

Code Availability

The Python code implementing the CNN-based regridding and QDM bias correction used to generate the CMIP6-MedPlus dataset is publicly available on GitHub at https://github.com/ValeriaTodaro/CMIP6-MedPlus.

Funding

This work was supported by OurMED PRIMA Program project funded by the European Union's Horizon 2020 research and innovation under grant agreement No. 2222. Valeria Todaro acknowledges financial support from the PNRR MUR project: ECS00000033ECOSISTER.

Author Contributions Statement

V.T. and D.S. contributed to conceptualization, data curation, formal analysis, methodology, and investigation. V.T. wrote the original draft of the manuscript, and D.S. contributed to manuscript review and editing. M.D. contributed to conceptualization, methodology, and investigation, and provided supervision and manuscript review and editing. M.G.T. contributed to conceptualization, manuscript review and editing, and supervision. All authors reviewed and approved the submitted manuscript.

Competing interests

The authors declare no competing interests.

References

Araya-Osses, D., Casanueva, A., Román-Figueroa, C., Uribe, J. M., and Paneque, M.: Climate change projections of temperature and precipitation in Chile based on statistical downscaling, Clim. Dyn., 54, 4309–4330, https://doi.org/10.1007/s00382-020-05231-4, 2020.

https://doi.org/10.5194/essd-2026-337
Preprint. Discussion started: 28 July 2026
© Author(s) 2026. CC BY 4.0 License.

Baño-Medina, J., Manzanas, R., and Gutiérrez, J. M.: Configuration and intercomparison of deep learning neural models for statistical downscaling, Geosci. Model Dev., 13, 2109–2124, https://doi.org/10.5194/gmd-13-2109-2020, 2020.

Baño-Medina, J., Manzanas, R., Cimadevilla, E., Fernández, J., González-Abad, J., Cofiño, A. S., and Gutiérrez, J. M.: Downscaling multi-model climate projection ensembles with deep learning (DeepESD): contribution to CORDEX EUR-44, Geosci. Model Dev., 15, 6747–6758, https://doi.org/10.5194/gmd-15-6747-2022, 2022.

Cannon, A. J., Sobie, S. R., and Murdock, T. Q.: Bias correction of GCM precipitation by quantile mapping: how well do methods preserve changes in quantiles and extremes?, J. Climate, 28, 6938–6959, https://doi.org/10.1175/JCLI-D-14-00754.1, 2015.

CORDEX: Second-order draft CORDEX experiment design for statistical downscaling of CMIP6, available at: https://cordex.org/wp-content/uploads/2024/04/Second-order-draft-CORDEX-experiment-design-for-statistical-downscaling-of-CMIP6.pdf (last access: 30 April 2026), 2024.

Eden, J. M. and Widmann, M.: Downscaling of GCM-simulated precipitation using model output statistics, J. Climate, 27, 312–324, https://doi.org/10.1175/JCLI-D-13-00063.1, 2014.

Eyring, V., Bony, S., Meehl, G. A., Senior, C. A., Stevens, B., Stouffer, R. J., and Taylor, K. E.: Overview of the Coupled Model Intercomparison Project Phase 6 (CMIP6) experimental design and organization, Geosci. Model Dev., 9, 1937–1958, https://doi.org/10.5194/gmd-9-1937-2016, 2016.

Fallah, B., Rostami, M., Russo, E., Harder, P., Menz, C., Hoffmann, P., Didovets, I., and Hattermann, F. F.: Climate model downscaling in central Asia: a dynamical and a neural network approach, Geosci. Model Dev., 18, 161–180, https://doi.org/10.5194/gmd-18-161-2025, 2025.

Fauzi, F., Kuswanto, H., and Atok, R. M.: Bias correction and statistical downscaling of earth system models using quantile delta mapping (QDM) and bias correction constructed analogues with quantile mapping reordering (BCCAQ), J. Phys.: Conf. Ser., 1538, 012050, https://doi.org/10.1088/1742-6596/1538/1/012050, 2020.

Fulton, D. J., Clarke, B. J., and Hegerl, G. C.: Bias correcting climate model simulations using unpaired image-to-image translation networks, Artificial Intelligence for the Earth Systems, 2, e220031, https://doi.org/10.1175/AIES-D-22-0031.1, 2023.

Giorgi, F. and Gutowski, W. J.: Regional dynamical downscaling and the CORDEX initiative, Annu. Rev. Environ. Resour., 40, 467–490, https://doi.org/10.1146/annurev-environ-102014-021217, 2015.

Giorgi, F. and Lionello, P.: Climate change projections for the Mediterranean region, Glob. Planet. Change, 63, 90–104, https://doi.org/10.1016/j.gloplacha.2007.09.005, 2008.

Gutiérrez, J. M., Maraun, D., Widmann, M., Huth, R., Hertig, E., Benestad, R., Rössler, O., Wibig, J., Wilcke, R., Kotlarski, S., San Martín, D., Herrera, S., Bedia, J., Casanueva, A., Manzanas, R., Iturbide, M., Vrac, M., Dubrovský, M., Ribalaygua,

https://doi.org/10.5194/essd-2026-337
Preprint. Discussion started: 28 July 2026
© Author(s) 2026. CC BY 4.0 License.

J., Pórtoles, J., Räty, O., Räisänen, J., Hingray, B., Raynaud, D., Casado, M. J., Ramos, P., Zerenner, T., Turco, M., Bosshard, T., Štěpánek, P., Bartholy, J., Pongrácz, R., Keller, D. E., Fischer, A. M., Cardoso, R. M., Soares, P. M. M., Czernecki, B., and Pagé, C.: An intercomparison of a large ensemble of statistical downscaling methods over Europe: results from the VALUE perfect predictor cross-validation experiment, Int. J. Climatol., 39, 3750–3785, https://doi.org/10.1002/joc.5462, 2019.

Gutowski, W. J., Jr., Giorgi, F., Timbal, B., Frigon, A., Jacob, D., Kang, H.-S., Raghavan, K., Lee, B., Lennard, C., Nikulin, G., O'Rourke, E., Rixen, M., Solman, S., Stephenson, T., and Tangang, F.: WCRP coordinated regional downscaling experiment (CORDEX): a diagnostic MIP for CMIP6, Geosci. Model Dev., 9, 4087–4095, https://doi.org/10.5194/gmd-9-4087-2016, 2016.

Harder, P., Hernandez-Garcia, A., Ramesh, V., Yang, Q., Sattegeri, P., Szwarcman, D., Watson, C., and Rolnick, D.: Hard-Constrained Deep Learning for Climate Downscaling, J. Mach. Learn. Res., 24, 1–40, 2023.

Hersbach, H., Bell, B., Berrisford, P., Hirahara, S., Horányi, A., Muñoz-Sabater, J., Nicolas, J., Peubey, C., Radu, R., Schepers, D., Simmons, A., Soci, C., Abdalla, S., Abellan, X., Balsamo, G., Bechtold, P., Biavati, G., Bidlot, J., Bonavita, M., De Chiara, G., Dahlgren, P., Dee, D., Diamantakis, M., Dragani, R., Flemming, J., Forbes, R., Fuentes, M., Geer, A., Haimberger, L., Healy, S., Hogan, R. J., Hólm, E., Janisková, M., Keeley, S., Laloyaux, P., Lopez, P., Lupu, C., Radnoti, G., de Rosnay, P., Rozum, I., Vamborg, F., Villaume, S., and Thépaut, J.-N.: The ERA5 global reanalysis, Q. J. R. Meteorol. Soc., 146, 1999–2049, https://doi.org/10.1002/qj.3803, 2020.

Huang, J., Zhang, J., Zhang, Z., Xu, C.-Y., Wang, B., and Yao, J.: Estimation of future precipitation change in the Yangtze River basin by using statistical downscaling method, Stoch. Environ. Res. Risk Assess., 25, 781–792, https://doi.org/10.1007/s00477-010-0441-9, 2011.

Intergovernmental Panel on Climate Change (IPCC): Climate Change 2021 – The Physical Science Basis, Working Group I Contribution to the Sixth Assessment Report of the Intergovernmental Panel on Climate Change, Cambridge University Press, https://doi.org/10.1017/9781009157896, 2023.

Jacob, D., Teichmann, C., Sobolowski, S., Katragkou, E., Anders, I., Belda, M., Benestad, R., Boberg, F., Buonomo, E., Cardoso, R. M., Casanueva, A., Christensen, O. B., Christensen, J. H., Coppola, E., De Cruz, L., Davin, E. L., Dobler, A., Dominguez, M., Fealy, R., Fernandez, J., Gaertner, M. A., Garcia-Diez, M., Giorgi, F., Gobiet, A., Goergen, K., Gomez-Navarro, J. J., González Alemán, J. J., Gutierrez, C., Gutiérrez, J. M., Guttler, I., Haensler, A., Halenka, T., Jerez, S., Jimenez-Guerrero, P., Jones, R. G., Keuler, K., Kjellström, E., Knist, S., Kotlarski, S., Maraun, D., van Meijgaard, E., Mercogliano, P., Montávez, J. P., Navarra, A., Nikulin, G., de Noblet-Ducoudré, N., Panitz, H.-J., Pfeifer, S., Piazza, M., Pichelli, E., Pietikäinen, J.-P., Prein, A. F., Preuschmann, S., Rechid, D., Rockel, B., Romera, R., Sanchez, E., Sieck, K., Soares, P. M. M., Somot, S., Srnec, L., Sørland, S. L., Termonia, P., Truhetz, H., Vautard, R., Warrach-Sagi, K., and Wulfmeyer, V.: Regional climate downscaling over Europe: perspectives from the EURO-CORDEX community, Reg. Environ. Change, 20, 1–20, https://doi.org/10.1007/s10113-020-01606-9, 2020.

https://doi.org/10.5194/essd-2026-337
Preprint. Discussion started: 28 July 2026
© Author(s) 2026. CC BY 4.0 License.
Earth System Science Data Discussions

Khazaei, M. R.: Performance comparison of four daily weather generators for historical period and downscaling future GCM scenarios, J. Water Clim. Change, 15, 5258–5271, https://doi.org/10.2166/wcc.2024.356, 2024.

Kingma, D. P. and Ba, J.: Adam: A method for stochastic optimization, arXiv [preprint], https://doi.org/10.48550/arXiv.1412.6980, 2014.

Labeurthre, D., Reffet, A., and Schrapffer, A.: An overview of statistical downscaling methods: techniques, applications, and advances, 2025.

LeCun, Y., Bengio, Y., and Hinton, G.: Deep learning, Nature, 521, 436–444, https://doi.org/10.1038/nature14539, 2015.

Lin, H., Tang, J., Wang, S., Wang, S., and Dong, G.: Deep learning downscaled high-resolution daily near-surface meteorological datasets over East Asia, Sci. Data, 10, 890, https://doi.org/10.1038/s41597-023-02805-9, 2023.

Maraun, D., Wetterhall, F., Ireson, A. M., Chandler, R. E., Kendon, E. J., Widmann, M., Brienen, S., Rust, H. W., Sauter, J., Themel, M., Venema, V. K. C., Chun, K. P., Goodess, C. M., Jones, R. G., Onof, C., Vrac, M., and Thiele-Eich, I.: Precipitation downscaling under climate change: recent developments to bridge the gap between dynamical models and the end user, Rev. Geophys., 48, RG3003, https://doi.org/10.1029/2009RG000314, 2010.

Maraun, D., Widmann, M., and Gutiérrez, J. M.: Statistical downscaling skill under present climate conditions: a synthesis of the VALUE perfect predictor experiment, Int. J. Climatol., 39, 3692–3703, https://doi.org/10.1002/joc.5877, 2019.

Maraun, D., Widmann, M., Gutiérrez, J. M., Kotlarski, S., Chandler, R. E., Hertig, E., Wibig, J., Huth, R., and Wilcke, R. A. I.: VALUE: a framework to validate downscaling approaches for climate change studies, Earth's Future, 3, 1–14, https://doi.org/10.1002/2014EF000259, 2015.

Maraun, D.: Bias correcting climate change simulations: a critical review, Curr. Clim. Change Rep., 2, 211–220, https://doi.org/10.1007/s40641-016-0050-x, 2016.

MedECC: Climate and Environmental Change in the Mediterranean Basin – Current Situation and Risks for the Future. First Mediterranean Assessment Report [Cramer, W., Guiot, J., and Marini, K. (eds.)], Union for the Mediterranean, Plan Bleu, UNEP/MAP, Marseille, France, 632 pp., ISBN 978-2-9577416-0-1, https://doi.org/10.5281/zenodo.4768833, 2020.

Menapace, A., Dhawan, P., Dalla Torre, D., Kaffas, K., Crespi, A., Larcher, M., Righetti, M., and Cannon, A. J.: Review of bias correction methods for climate model outputs in hydrology, J. Hydrol., 660, 133213, https://doi.org/10.1016/j.jhydrol.2025.133213, 2025.

Noël, T., Loukos, H., Defrance, D., Vrac, M., and Levavasseur, G.: A high-resolution downscaled CMIP5 projections dataset of essential surface climate variables over the globe coherent with the ERA5 reanalysis for climate change impact assessments, Data Brief, 35, 106900, https://doi.org/10.1016/j.dib.2021.106900, 2021.

https://doi.org/10.5194/essd-2026-337
Preprint. Discussion started: 28 July 2026
© Author(s) 2026. CC BY 4.0 License.

O'Neill, B. C., Kriegler, E., Ebi, K. L., Kemp-Benedict, E., Riahi, K., Rothman, D. S., van Ruijven, B. J., van Vuuren, D. P., Birkmann, J., Kok, K., Levy, M., and Solecki, W.: The roads ahead: narratives for shared socioeconomic pathways describing world futures in the 21st century, Glob. Environ. Change, 42, 169–180, https://doi.org/10.1016/j.gloenvcha.2015.01.004, 2017.

O'Neill, B. C., Tebaldi, C., van Vuuren, D. P., Eyring, V., Friedlingstein, P., Hurtt, G., Knutti, R., Kriegler, E., Lamarque, J.-F., Lowe, J., Meehl, G. A., Moss, R., Riahi, K., and Sanderson, B. M.: The Scenario Model Intercomparison Project (ScenarioMIP) for CMIP6, Geosci. Model Dev., 9, 3461–3482, https://doi.org/10.5194/gmd-9-3461-2016, 2016.

Piani, C., Weedon, G. P., Best, M., Gomes, S. M., Viterbo, P., Hagemann, S., and Haerter, J. O.: Statistical bias correction of global simulated daily precipitation and temperature for the application of hydrological models, J. Hydrol., 395, 199–215, https://doi.org/10.1016/j.jhydrol.2010.10.024, 2010.

Pierce, D. W., Cayan, D. R., Maurer, E. P., Abatzoglou, J. T., and Hegewisch, K. C.: Improved bias correction techniques for hydrological simulations of climate change, J. Hydrometeorol., 16, 2421–2442, https://doi.org/10.1175/JHM-D-14-0236.1, 2015.

Rampal, N., Gibson, P. B., Sood, A., Stuart, S., Fauchereau, N. C., Brandolino, C., Noll, B., and Meyers, T.: High-resolution downscaling with interpretable deep learning: rainfall extremes over New Zealand, Weather Clim. Extremes, 38, 100525, https://doi.org/10.1016/j.wace.2022.100525, 2022.

Ruti, P. M., Somot, S., Giorgi, F., Dubois, C., Flaounas, E., Obermann, A., Dell'Aquila, A., Pisacane, G., Harzallah, A., Lombardi, E., Ahrens, B., Akhtar, N., Alias, A., Arsouze, T., Aznar, R., Bastin, S., Bartholy, J., Béranger, K., Beuvier, J., Bouffies-Cloche, S., Brauch, J., Cabos, W., Calmanti, S., Calvet, J.-C., Carillo, A., Conte, D., Coppola, E., Djurdjevic, V., Drobinski, P., Elizalde-Arellano, A., Gaertner, M., Galán, P., Gallardo, C., Gualdi, S., Goncalves, M., Jorba, O., Jordà, G., L'Heveder, B., Lebeaupin-Brossier, C., Li, L., Liguori, G., Lionello, P., Maciàs, D., Nabat, P., Önol, B., Raikovic, B., Ramage, K., Sevault, F., Sannino, G., Struglia, M. V., Sanna, A., Torma, C., and Vervatis, V.: Med-CORDEX initiative for Mediterranean climate studies, Bull. Am. Meteorol. Soc., 97, 1187–1208, https://doi.org/10.1175/BAMS-D-14-00176.1, 2016.

Schmidli, J., Frei, C., and Vidale, P. L.: Downscaling from GCM precipitation: a benchmark for dynamical and statistical downscaling methods, Int. J. Climatol., 26, 679–689, https://doi.org/10.1002/joc.1287, 2006.

Serifi, A., Günther, T., and Ban, N.: Spatio-Temporal Downscaling of Climate Data Using Convolutional and Error-Predicting Neural Networks, Front. Clim., 3, 656479, https://doi.org/10.3389/fclim.2021.656479, 2021.

Sharma, S. C. M., Kumar, B., Mitra, A., and Saha, S. K.: Deep learning-based bias correction of ISMR simulated by GCM, Atmos. Res., 309, 107589, https://doi.org/10.1016/j.atmosres.2024.107589, 2024.

https://doi.org/10.5194/essd-2026-337
Preprint. Discussion started: 28 July 2026
© Author(s) 2026. CC BY 4.0 License.

Soares, P. M. M., Johannsen, F., Lima, D. C. A., Lemos, G., Bento, V. A., and Bushenkova, A.: High-resolution downscaling of CMIP6 Earth system and global climate models using deep learning for Iberia, Geosci. Model Dev., 17, 229–259, https://doi.org/10.5194/gmd-17-229-2024, 2024.

Sobolowski, S., Somot, S., Fernandez, J., Evin, G., Maraun, D., Kotlarski, S., Jury, M., Benestad, R. E., Teichmann, C., Christensen, O. B., Bülow, K., Buonomo, E., Katragkou, E., Steger, C., Sørland, S., Nikulin, G., McSweeney, C., Dobler, A., Palmer, T., Wilke, R., Boé, J., Brunner, L., Ribes, A., Qasmi, S., Nabat, P., Sevault, F., Oudar, T., and Brands, S.: EURO-CORDEX GCM Selection & Ensemble Design: Implementation Framework, Zenodo, https://doi.org/10.5281/zenodo.7673400, 2023.

Sun, Y., Deng, K., Ren, K., Liu, J., Deng, C., and Jin, Y.: Deep learning in statistical downscaling for deriving high spatial resolution gridded meteorological data: a systematic review, ISPRS J. Photogramm. Remote Sens., 208, 14–38, https://doi.org/10.1016/j.isprsjprs.2023.12.011, 2024.

Tabari, H., Paz, S. M., Buekenhout, D., and Willems, P.: Comparison of statistical downscaling methods for climate change impact analysis on precipitation-driven drought, Hydrol. Earth Syst. Sci., 25, 3493–3517, https://doi.org/10.5194/hess-25-3493-2021, 2021.

Teutschbein, C. and Seibert, J.: Bias correction of regional climate model simulations for hydrological climate-change impact studies: review and evaluation of different methods, J. Hydrol., 456–457, 12–29, https://doi.org/10.1016/j.jhydrol.2012.05.052, 2012.

Themeßl, M. J., Gobiet, A., and Heinrich, G.: Empirical-statistical downscaling and error correction of regional climate models and its impact on the climate change signal, Climatic Change, 112, 449–468, https://doi.org/10.1007/s10584-011-0224-4, 2012.

Tian, D. and Martinez, C. J.: Comparison of two analog-based downscaling methods for regional reference evapotranspiration forecasts, J. Hydrol., 475, 350–364, https://doi.org/10.1016/j.jhydrol.2012.10.009, 2012.

Tian, D., Martinez, C. J., Graham, W. D., and Hwang, S.: Statistical downscaling multimodel forecasts for seasonal precipitation and surface temperature over the southeastern United States, J. Climate, 27, 8384–8411, https://doi.org/10.1175/JCLI-D-13-00481.1, 2014.

Todaro, V., D'Oria, M., Secci, D., Zanini, A., and Tanda, M. G.: Climate change over the Mediterranean region: local temperature and precipitation variations at five pilot sites, Water, 14, 2499, https://doi.org/10.3390/w14162499, 2022.

Todaro, V., Secci, D., D'Oria, M., and Tanda, M. G.: CMIP6-MedPlus: downscaled climate projections for the Mediterranean region [data set]. Zenodo. https://doi.org/10.5281/zenodo.17898529, 2025.

https://doi.org/10.5194/essd-2026-337
Preprint. Discussion started: 28 July 2026
© Author(s) 2026. CC BY 4.0 License.

Tong, Y., Gao, X., Han, Z., Xu, Y., Xu, Y., and Giorgi, F.: Bias correction of temperature and precipitation over China for RCM simulations using the QM and QDM methods, Clim. Dyn., 57, 1425–1443, https://doi.org/10.1007/s00382-020-05447-4, 2021.

Tuel, A. and Eltahir, E. A. B.: Why is the Mediterranean a climate change hot spot?, J. Climate, 33, 5829–5843, https://doi.org/10.1175/JCLI-D-19-0910.1, 2020.

Wang, F. and Tian, D.: Multivariate bias correction and downscaling of climate models with trend-preserving deep learning, Clim. Dyn., 62, 9651–9672, https://doi.org/10.1007/s00382-024-07406-9, 2024.

Widmann, M., Bretherton, C. S., and Salathé, E. P.: Statistical precipitation downscaling over the northwestern United States using numerically simulated precipitation as a predictor, J. Climate, 16, 799–816, https://doi.org/10.1175/1520-0442(2003)016<0799:SPDOTN>2.0.CO;2, 2003.

Wilby, R. L., Wigley, T. M. L., Conway, D., Jones, P. D., Hewitson, B. C., Main, J., and Wilks, D. S.: Statistical downscaling of general circulation model output: a comparison of methods, Water Resour. Res., 34, 2995–3008, https://doi.org/10.1029/98WR02577, 1998.

Wilks, D. S. and Wilby, R. L.: The weather generation game: a review of stochastic weather models, Prog. Phys. Geogr., 23, 329–357, https://doi.org/10.1177/030913339902300302, 1999.

Xavier, A. C. F., Martins, L. L., Rudke, A. P., de Morais, M. V. B., Martins, J. A., and Blain, G. C.: Evaluation of Quantile Delta Mapping as a bias-correction method in maximum rainfall dataset from downscaled models in São Paulo state (Brazil), Int. J. Climatol., 42, 175–190, https://doi.org/10.1002/joc.7238, 2022.

Zhang, F.-Y., Liu, Y.-X., Li, X.-B., Wang, X., Tan, M.-H., and Xin, L.-J.: Downscaling daily climate data with super-resolution and CMIP6 global climate models to predict the climate in China, Adv. Clim. Change Res., 17, 79–90, https://doi.org/10.1016/j.accre.2025.11.007, 2026.

Zhuang, J., dussin, r., Huard, D., Bourgault, P., Banihirwe, A., Raynaud, S., Malevich, B., Schupfner, M., Filipe, Gauthier, C., Levang, S., Jüling, A., Almansi, M., RichardScottOZ, RondeauG, Rasp, S., Smith, T. J., Mares, B., Stachelek, J., Plough, M., Pierre, Bell, R., Caneill, R., and Li, X.: pangeo-data/xESMF: v0.8.8, Zenodo [code], https://doi.org/10.5281/zenodo.14025505, 2024.

Zorita, E. and von Storch, H.: The analog method as a simple statistical downscaling technique: comparison with more complicated methods, J. Climate, 12, 2474–2489, https://doi.org/10.1175/1520-0442(1999)012<2474:TAMAAS>2.0.CO;2, 1999.

Şan, M., Nacar, S., Kankal, M., and Bayram, A.: Daily precipitation performances of regression-based statistical downscaling models in a basin with mountain and semi-arid climates, Stoch. Environ. Res. Risk Assess., 37, 1431–1455, https://doi.org/10.1007/s00477-022-02345-5, 2023.